ACSNANO
www.acsnano.org
ARTICLE

Tribotronic Transistor Array as an Active Tactile Sensing System

Zhi Wei Yang,[†] Yaokun Pang,[†] Limin Zhang,[†] Cunxin Lu,[†] Jian Chen,[†] Tao Zhou,[†] Chi Zhang,*[,†] and Zhong Lin Wang*[,†,‡]

[†]Beijing Institute of Nanoenergy and Nanosystems, Chinese Academy of Sciences, and National Center for Nanoscience and Technology (NCNST), Beijing 100083, P. R. China

[‡]School of Materials Science and Engineering, Georgia Institute of Technology, Atlanta, Georgia 30332, United States

Supporting Information

ABSTRACT: **Large-scale tactile sensor arrays are of great importance in flexible electronics, human−robot interaction, and medical monitoring. In this paper, a flexible 10 × 10 tribotronic transistor array (TTA) is developed as an active tactile sensing system by incorporating field-effect transistor units and triboelectric nanogenerators into a polyimide substrate. The drain−source current of each tribotronic transistor can be individually modulated by the corresponding external contact, which has induced a local electrostatic potential to act as the conventional gate voltage. By scaling down the pixel size from 5 × 5 to 0.5 × 0.5 mm^2, the sensitivities of single pixels are systematically investigated. The pixels of the TTA show excellent durability, independence, and synchronicity, which are suitable for applications in real-time tactile sensing, motion monitoring, and spatial mapping. The integrated tribotronics provides an unconventional route to realize an active tactile sensing system, with prospective applications in wearable electronics, human−machine interfaces, fingerprint identification, and so on.**

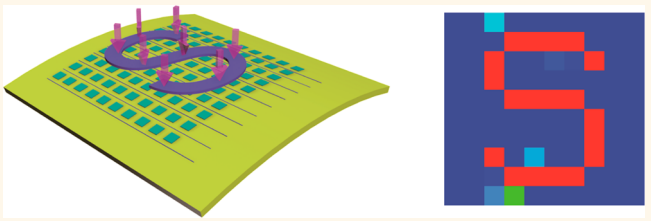

KEYWORDS: *tribotronics, TENG, tactile sensor, motion monitoring, spatial mapping*

As a key technique in the intelligent sensing field, tactile sensors have been extensively used to detect external stimuli and imitate tactile perception.[1−3] Inspired by the huge potentials in smart wearable devices, human−machine interfaces, and real-time healthcare monitoring, considerable attention has been continuously focused on the tactile sensor, and tremendous progress has been achieved in recent years.[4−19] Different physical transduction mechanisms including conductance,[9] resistance,[11−13] capacitance,[14] waveguide,[20] magnetism,[21,22] piezoelectricity,[10,23] and piezoresistivity[24] have been utilized to fabricate these tactile sensors. Meanwhile, active interaction between mechanical stimuli and electronics remains challenging for most tactile sensing systems, possibly due to cost and complexity of integration.[15−19,24−27] Therefore, developing a large-scale, low-cost, commercialized, and active tactile sensor is highly desired.

The newly arising technology of triboelectric nanogenerators (TENGs) developed by Wang *et al.* could be a promising candidate to address the issues mentioned above.[28−30] The TENG can harvest ambient mechanical energy and convert it into electricity, which has been directly used as self-powered active sensors.[31−37] Meanwhile, the electrostatic potential created by the TENG can serve as a gate voltage to modulate electronic devices, which has opened up a new research field of tribotronics.[38] Such tribo-controlled devices have demonstrated applications including tribotronic transistors,[39,40] microelectrochemical systems,[41] logic circuits,[42] memory devices,[43] organic light-emitting diodes,[44] phototransistors,[45,46] and tactile switches.[47] Tribotronics has offered a prospective strategy to design a novel active tactile sensing system with advantages of low cost, simple mechanism, and easy process.

In this work, a large-scale, active, and high-sensitivity tribotronic transistor array (TTA) as an active tactile sensing system is presented by a facile and inexpensive approach. Other than traditional gate voltage, the transistor unit of the TTA is gated by external stimuli, which acts as a sensing element by virtue of the change of the drain−source current (I_{DS}). The flexible substrate-based high-performance TTA has been successfully utilized to realize multipoint tactile sensing, dynamic motion monitoring, real-time trajectory recording, and external stimuli spatial mapping while keeping excellent sensitivity and long-term stability. The TTA coupled by traditional integrated circuits with triboelectrification has illustrated its potential in active tactile sensing systems and next-generation wearable device applications.

Received: August 15, 2016
Accepted: November 18, 2016
Published: November 18, 2016

DOI: 10.1021/acsnano.6b05507
ACS Nano XXXX, XXX, XXX−XXX

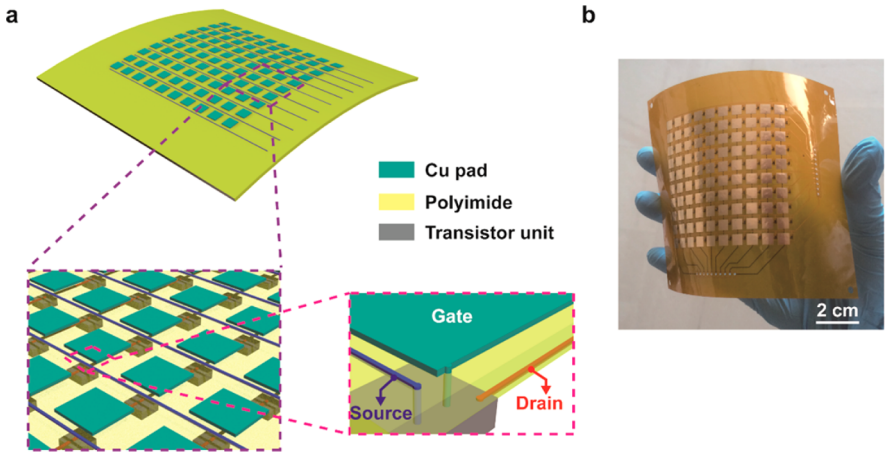

Figure 1. Structure of the TTA. (a) Schematic of a 10 × 10 TTA. Insets: Partial enlarged tilted views of the TTA configuration and pixel structure, respectively. (b) Optical photograph of a fully integrated TTA with each sensing pixel of 5 × 5 mm^2.

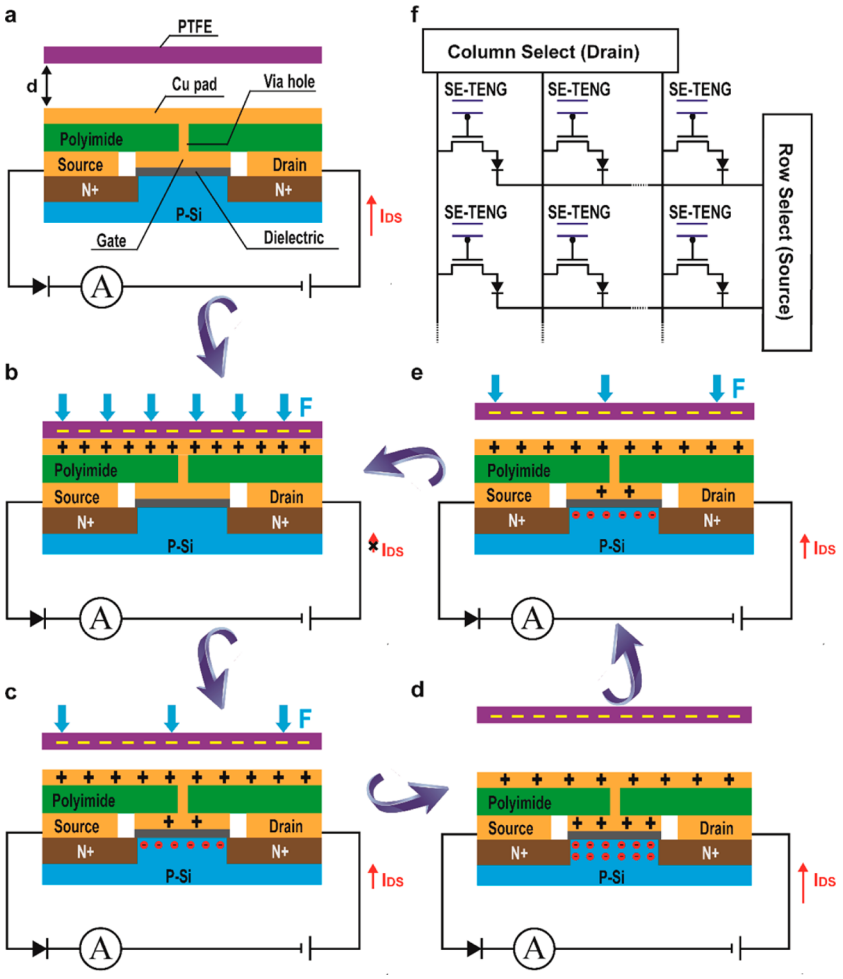

Figure 2. Schematic representations of the working principle for a single pixel and the equivalent circuit schematic of TTA. (a) Sketch of a single pixel. (b–e) Change of the conduction channel width and resulting drain–source current (I_{DS}) when the PTFE layer contacts with and separates from the Cu pad. (f) Equivalent circuit schematic of the active tactile sensing system.

RESULTS AND DISCUSSION

Structure of the TTA. A schematic structure of the 10 × 10 TTA is depicted in Figure 1a. Each pixel with a size of 5 × 5 mm^2, composed of a square Cu pad and a transistor unit, is integrated on the top and bottom layer of a flexible polyimide substrate (the fabrication processes of TTA are described in detail in the Methods). The gate electrode of the transistor is electrically connected to the Cu pad by the via hole. The drain electrodes of the 10 transistors in every column are commonly connected to an electrical wire, so are the source electrodes of those in every row. By selecting a column electrical wire, the corresponding 10 pixels between this wire and the row

DOI: 10.1021/acsnano.6b05507
ACS Nano XXXX, XXX, XXX–XXX

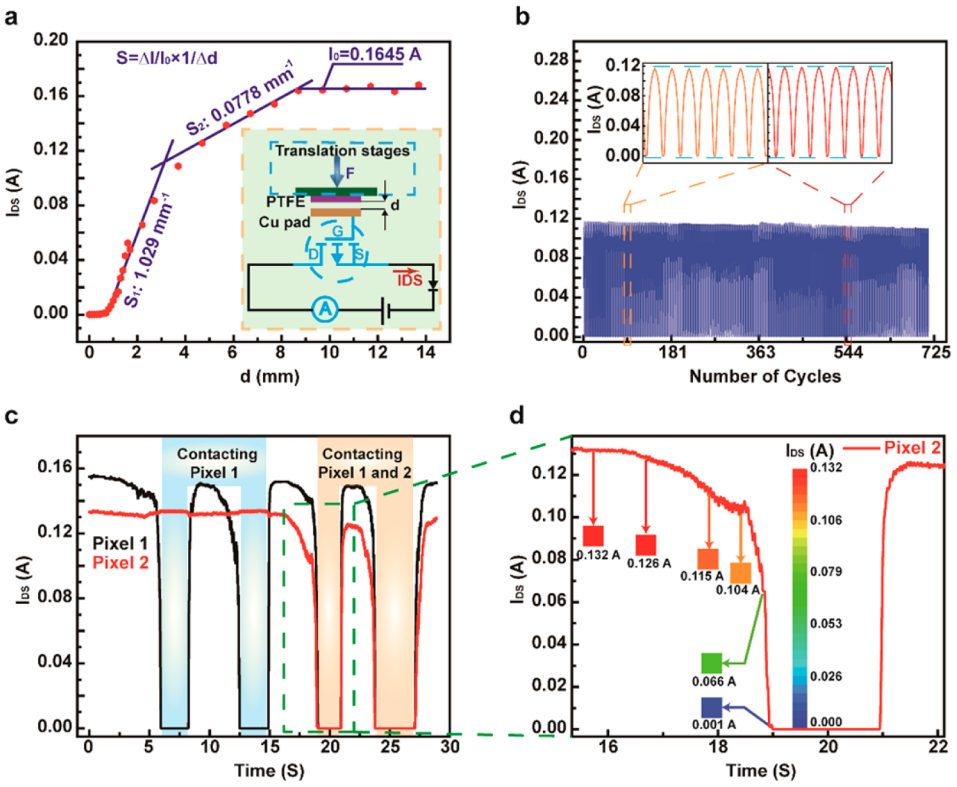

Figure 3. Electrical characterization of single sensing pixel in TTA. (a) Sensitivity of the pixel, represented by an output current as a function of separation distance. An ultrahigh sensitivity of 1.029 mm^{-1} is obtained below 3 mm and sharply declines to 0.0778 mm^{-1} in the range of 3–9 mm. Inset: Schematic illustration of the sensitivity test of the pixel. (b) Durability test for more than 700 contact–separation cycles, demonstrating the excellent performance of the sensing device with negligible current degradation. Inset: Comparison of current characteristics of two enlarged areas. (c) Output current characteristics of two pixels in individual and simultaneous contact–separation process to demonstrate their independence and synchronicity characteristics. (d) Partial enlarged view of the current characteristic, showing the gradual change trend of the I_{DS} of a single pixel in the temporal domain and its color display.

electrical wires can be individually addressable. A photograph of a well-designed TTA with good electrical contact is shown in Figure 1b with a resolution of 5 dpi.

Principle of the TTA. Based on the coupling effects of the transistor and contact electrification, the working principle of the TTA is demonstrated with cross-sectional and equivalent circuit schematics in Figure 2. The transistor unit consists of an n-type transistor and a diode, in which the source electrode of the transistor is interconnected with the anode of the diode. This configuration ensures the current flows through the transistor in only one direction. In the original state (Figure 2a), a polytetrafluoroethylene (PTFE) film is prepared to serve as the mobile friction layer for contact electrification, which can approach and separate from the Cu pad by an external force. Since the PTFE is triboelectrically more negative than Cu, when the PTFE film is forced to fully contact with the Cu pad, equal negative and positive charges can be induced on the surfaces of the PTFE film and the Cu pad, respectively (Figure 2b). At this moment, there is no conduction channel between the source and drain electrode, hence generating little I_{DS}. When the PTFE film is gradually separated from the Cu pad (Figure 2c), an electric field and a potential drop are created due to the electrostatic induction and the edge electric field leakage from the finite size Cu pad and PTFE film, resulting in a built-in voltage at the gate electrode and generating an inversion conduction channel that enables electrons to flow freely between the drain and source electrodes. Under this circumstance, the I_{DS} can be produced with an applied drain–source voltage (V_{DS}). Further increase of the separation distance is equivalent to enhancing the gate voltage (V_{GS}), which can lead to the increase of the conduction channel width and thus an evidently increased I_{DS}. Predictably, once the separation distance increases to a threshold (Figure 2d), the triboelectric-charge-induced gate voltage and resulting current will remain stable at a maximum value if the PTFE film continues to be moved vertically away from the Cu pad. When the mobile PTFE film is pressed to approach the Cu pad again (Figure 2e), recovery of the I_{DS} can be observed. In the whole process, the I_{DS} of the transistor is able to be tuned by the externally physical access/contact, in place of the electrically applied gate voltage.

As can be seen from the equivalent circuit diagram of the TTA in Figure 2f, each pixel is addressed individually by a corresponding single-electrode TENG (SE-TENG). Compared to sensor arrays with every pixel grounded or addressed individually,[2,9,14,32,34] a distinct advantage of a $p \times q$ TTA is that the addressing lines have been greatly reduced from $p \times q$ to $p + q$. This reduction is also attributed to the addition of a diode in each pixel, which enables the unidirectional flow of I_{DS} in the pixel without any interference of other pixels. In this case, the complex electrical connection of the TTA has been significantly simplified to 20 addressing lines, thus obviously enhancing the addressing speed and facilitating future development of a large-area TTA with simplified but effective electrical connection.

DOI: 10.1021/acsnano.6b05507
ACS Nano XXXX, XXX, XXX–XXX

Characteristics of the Single Sensing Pixel in TTA. To evaluate the sensing characteristics of the TTA, the distance-dependent performance of a single pixel was precisely determined by manual translation stages. The sensitivity of the TTA is defined as

$$S = (\Delta I/I_0)/\Delta d \quad (1)$$

where ΔI is the relative change in the I_{DS}, I_0 is the initial current of the pixel without external stimuli, and Δd is the distance change between the PTFE film and the Cu pad. To quantify the parameter distance, the fully physical contact state between the PTFE film and the Cu pad was selected as the initial position. When the PTFE film was moved outward by an external force, the distance increased. Figure 3a shows the current response of the pixel to the distance, and the schematic illustration of the sensitivity test is shown in the inset. Initially, the pixel displayed a high sensitivity of 1.029 mm^{-1} even with a slight distance increase. However, once the PTFE film surpassed a "critical distance" of 3 mm, a remarkable sensitivity decrease of more than an order of magnitude could be observed. As the distance continued to increase, the output current finally saturated and the pixel would no longer be sensitive to the distance change. Once the PTFE film was forced to approach and ultimately contact with the Cu pad again, an inverse process would be seen. The whole process could be ascribed to the triboelectric charge redistribution in the gate electrode of the pixel, which has been elaborated in its working mechanism presented in Figure 2.

In order to comprehensively analyze the influence of the separation distance on the triboelectric-charge-induced V_{GS} and the modulated I_{DS}, a finite-element simulation was performed using COMSOL to illustrate the potential distribution at the gate electrode of the tribotronic transistor (Figures S1 and S2). Besides this simulation, output and transfer characteristic curves of a representative transistor were measured and depicted (Figure S3a shows the output characteristic of the transistor, and transfer curves in linear, log and root square scale are provided in Figure S3b–d, respectively). Based on the established model that a PTFE film separated from and approached a Cu pad, which was electrically connected to the gate electrode of a transistor, the exact same geometry parameters were utilized to obtain an accurate result. The PTFE film (25 μm thick) had a size of 5 × 5 mm^2, so did the Cu pad (10 μm in thickness). The charge density was assumed to be −10 $\mu C\ m^{-2}$ on the contacting surface of the PTFE film and +10 $\mu C\ m^{-2}$ on the surface of the Cu pad. The distance between the PTFE film and the Cu pad ranged from 0 to 12 mm. One point that should be emphasized was that changes in these assumed parameters aforementioned would only affect the magnitude of the result and not the changing trend. After making these assumptions, electric potential distribution (d = 0.2, 1, 2, 4, 6, 10, and 12 mm) at the gate electrode was simulated and is presented in Figure S1. It indicated an increasing trend of the V_{GS} with the increase of the separation distance. When d increased from 0 to 12 mm, the corresponding V_{GS} increased from 0 to 4.74 V. Besides this result, the relationship between the triboelectric-charge-induced V_{GS} and separation distance was also calculated and graphed in Figure S2. As the distance grew continually, the V_{GS} exhibited a slower growth over 3 mm. This phenomenon could be very persuasive because a similar trend was found in Figure 3a and Figures S2 and S3a. When the separation distance kept growing (or the V_{GS}), a relative slow growth of the I_{DS} could be clearly observed. Convincingly, these results proved the relationship between the separation distance and the I_{DS} of the transistor. To sum up, the simulated analysis in Figures S1 and S2, along with the transfer and output curves in Figure S3, which was in good agreement with the measured results in Figure 3a, further confirmed the validity of employing the external force to substitute the electrical gate voltage and realize the modulation of I_{DS} via the change of electrostatic potential.

According to previous studies,[34,48,49] the induced electrostatic potential has a close relation with the amount of transferred charges. To better understand the influence of Cu pad size in the sensitivity and acquire a possibly high resolution of the TTA, the sensitivities of single pixel with different sizes were systematically investigated. As shown in Figure S4, the I_{DS}–distance curves of four pixels with corresponding Cu pad area varying from 4 × 4 to 0.5 × 0.5 mm^2 were obtained, and they provided a clear view of the pixel sensitivity changes. Three typical regions of sensitivity could be found in each figure, which was in good agreement with the result in Figure 3a. The experimental results indicated that, as the pixel size diminished, the corresponding sensitivity also declined both in high- and low-sensitivity regions. It was noteworthy that, in Figure S4d, the pixel with its size of 0.5 × 0.5 mm^2 displayed distinguishable sensitivities of 0.116 and 0.0085 mm^{-1} (according to the defined sensitivity in eq 1) in two different regions even if the I_{DS} was unable to decrease to zero when the PTFE film moved to fully contact the Cu pad. This result could be attributable to the diminished area of the contact Cu pad and proportionately decreased electrostatic charges, as previous research has demonstrated. Due to the shrunken area of the Cu pad, the edge electric leakage would be more distinct, which leads to a higher proportion of triboelectric charges on the Cu pad transferred to the gate electrode. Nevertheless, since the area of the Cu pad was reduced more rapidly, in fact, the amount of the total charges transferred diminished. Meanwhile, the transistors used in all experiments were maintained the same and had the same characteristics to be gated. Consequently, as the area of the Cu pad shrank, a poorer sensing performance was observed in Figure S4a–d. In Figure S4d, the Cu pad size was 100 times smaller than that in Figure 3a, causing the created electrostatic potential to be insufficient to shut down the conduction channel. Hence, the I_{DS} could remain above zero when the distance returned to the "fully physical contact state". Due to this result, a square pixel with 0.5 mm length size and good sensitivity was used as the smallest pixel in our research, realizing a resolution of about 50 dpi.

Response time of the pixel is another essential sensing feature of the TTA. In Figure S5a, the pixel exhibited a rapid response to the external stimuli during a quick contact–separation process. The measured response and recovery times, as illustrated in Figure S5b, were ∼78 and ∼86 ms, respectively, which should be sufficiently fast for practical applications. Moreover, a durability test was conducted at a constant V_{DS} of 2 V for more than 700 contact–separation cycles, as demonstrated in Figure 3b. The output current showed no apparent signal shift or degradation during the test, proving the TTA can provide reproducible and reliable external tactile perception.

Furthermore, to investigate whether pixels in the TTA can function well individually and simultaneously, two pixels were selected and electrical characteristics were determined, as plotted in Figure 3c. In the beginning, no PTFE film touched the two pixels, and they exhibited relatively stable, though

DOI: 10.1021/acsnano.6b05507
ACS Nano XXXX, XXX, XXX–XXX

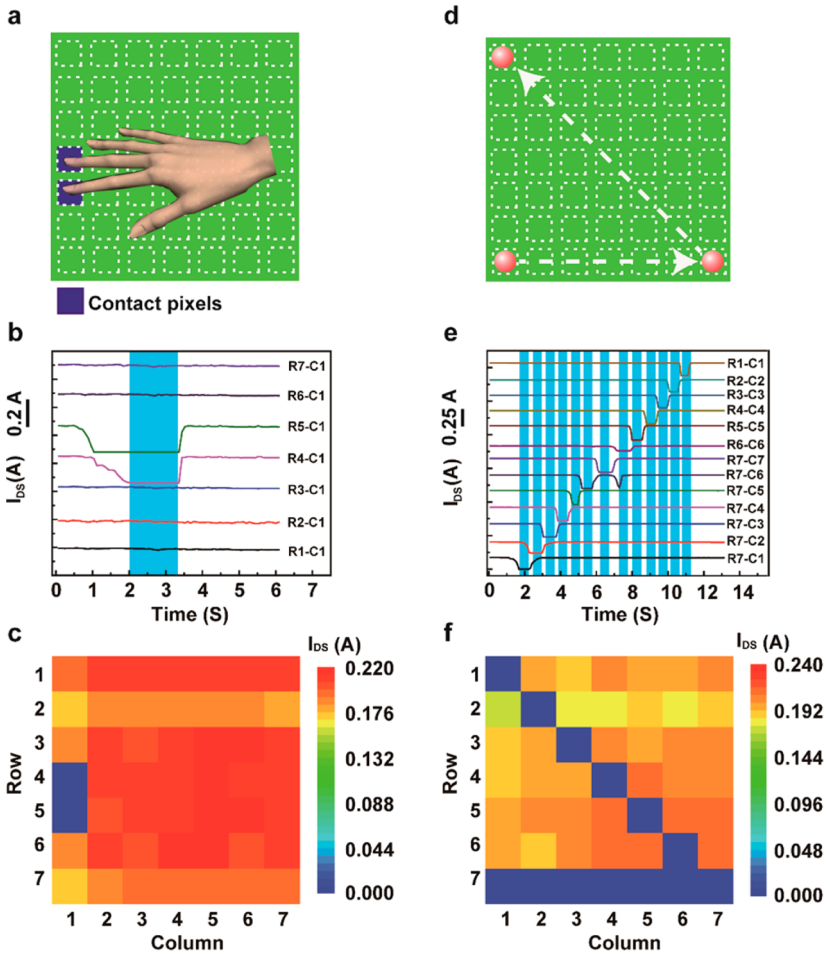

Figure 4. TTA for multipoint tactile sensing and motion monitoring. (a) Schematic illustration of two-point contact. (b) Output currents of pixels in the first column measured by multichannel measurement system. (c) Corresponding current signals plotted as two-dimensional intensity map. (d) Schematic of a ball moving along different pixels. (e) Output currents of pixels in the moving trajectory of the ball. (f) Two-dimensional intensity map reconstructed from (e) with the measured current signals during the ball moving.

slightly different, I_{DS}. At nearly 3 s, a PTFE film slowly approached pixel 1, and the corresponding I_{DS} of pixel 1 showed a slow rate of decrease. From 5.5 s, decreasing the distance to fully contact the Cu pad dramatically reduced the current by more than 4 orders of magnitude to almost zero in less than 0.5 s, which could be supported in Figure 3a. In the meantime, pixel 2 presented a nearly unvaried I_{DS}, proving that it was not influenced and each pixel could work independently. Then, as the PTFE film touched both pixels, similar decreasing trends of the I_{DS} were obtained, which strongly supported that pixels could work synchronously. It should also be mentioned in this experiment that, though there were variations in I_{DS} among different pixels, only the magnitude of I_{DS} was affected, not the decreasing or increasing trend. Another factor that should be taken into account is that the output current signal initially experienced a gradual change and then a fast trend of decrease, as depicted in the color display in Figure 3d. This phenomenon is of great importance because it exhibits that the I_{DS} has a different responsive extent according to varying distance between the PTFE film and the Cu pad, signifying that the TTA can be constructed to resolve gradual changes in responding to external access. Owing to the excellent sensing capabilities, these sensing pixels are suitable for large-scale integration into a flexible substrate and have a widespread range of applications, such as tactile sensing, e-skins, and healthcare monitoring.

Application of the TTA for Active Tactile Sensing. In order to fulfill TTA's potential in active tactile sensing applications, these sensor pixels are integrated into a sensing device system, which provides a touch−user interface, enabling the tactile profile, dynamic motion, and trajectory to be spatially mapped. As an illustration, a flexible 7 × 7 TTA was fabricated. All output current signals were acquired via the multichannel data acquisition system. Figure 4a is a schematic illustration of two-point contact, and Figure 4b shows the measured I_{DS} in the first column pixels of the TTA. An evident current fall of pixel R4-C1 and pixel R5-C1 could be seen, while other pixels maintained their I_{DS} unchanged. According to the measured current signals, a reconstructed intensity map of all pixels, with colors representing the output current signal for each pixel, is demonstrated in Figure 4c and the two contact pixels were precisely identified (a short video demonstrating the multipoint sensing process is provided in Video S1, Supporting Information). Besides multipoint identification, monitoring the motion and recording the trajectory of moving objects also demonstrated the intriguing features of the TTA. As a PTFE film (5 × 5 mm^2 area) moved along the last row and then the diagonal of the TTA, the trajectory profile could be clearly recorded in real-time and plotted as a two-dimensional

DOI: 10.1021/acsnano.6b05507
ACS Nano XXXX, XXX, XXX−XXX

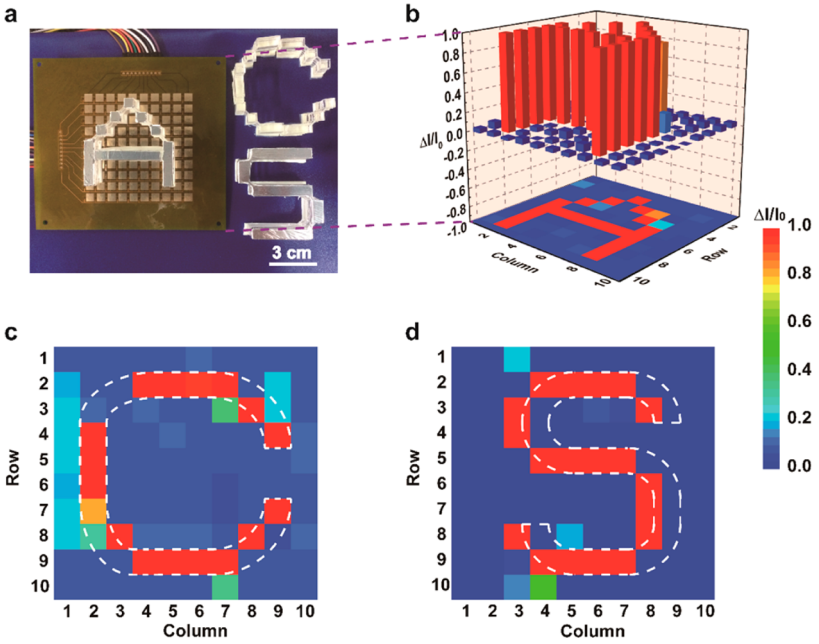

Figure 5. TTA as a fully integrated system for tactile sensing and map reconstruction. (a) Photograph of a 10 × 10 TTA with three as-fabricated letter-shaped acrylic slabs placed on the surface of its sensing area. (b) Corresponding three-dimensional and two-dimensional normalized I_{DS} intensity map of the A-shaped letter. (c,d) Normalized two-dimensional intensity profile of current signal for the shape of "C" and "S" reconstructed by the tactile sensing system.

intensity graph, shown in Figure 4f (a ball was used to substitute the PTFE film for demonstration in Figure 4d). Apparently, a motion path, first moving from pixel R7-C1 to pixel R7-C7 and then from pixel R7-C7 to pixel R1-C1 diagonally, was distinguished in the graph, which was in good accord with the current signal change of pixels depicted in Figure 4e (videos of the motion monitoring and trajectory recording experiment are provided in Video S2 and Video S3 in the Supporting Information). Notably, two current falls were observed in the I_{DS} response of pixel R7-C6 in Figure 4e, and the second one could be explained by the turning of the moving ball to the diagonal direction, which placed the ball close to pixel R7-C6 again. Therefore, these experiments validate that TTA has good practicability for multipoint sensing, dynamic movement monitoring, and trajectory tracking because of its relatively high measurement precision and real-time tracing ability.

Additionally, the sensing ability of the active tactile sensing system has been further accessed by placing letter-shaped slabs onto the sensing pixels of a flexible 10 × 10 TTA. Here, as presented in Figure 5a, the PTFE films clinging to C-, A-, and S-shaped acrylic slabs were prepared. A layer of elastic sponge was sandwiched between the PTFE film and the acrylic slab to ensure the uniform distribution of pressure over an area corresponding to the predesigned PTFE slabs. Before placing these "letters" on the sensing area, a background mapping had been accomplished in advance to serve as a reference, shown in Figure S6a (V_{DS} = 2 V). The I_{DS} distribution map showed good uniformity in electrical characteristics among all 100 pixels, with 94% of the output current values in the narrow range of 0.105 ± 0.009 A. Obvious current variations found in pixels like pixel R10-C3 and pixel R10-C4 could mainly be the result of different amounts of induced charges on the Cu pad after the initial contact with the PTFE film. For the purpose of minimizing the interference of current variations among pixels, the ratio of ΔI to I_0 was used to reconstruct the intensity image (a two-dimensional intensity map of measured I_{DS} in the shape of letter "A" is provided in Figure S6b, Supporting Information), and Figure 5b–d displays the reconstructions of the "letter" image and clearly shows that pixels contacting the slabs experienced the greatest relative current changes, except for some pixels such as pixel R3-C3 and pixel R7-C2 in Figure 5c. This phenomenon could be caused by the uneven surface of the PTFE film, which resulted in pixels that failed to touch the film and hence was unable to induce enough electrostatic charges to tune the I_{DS}. To eliminate such defective pixels, the performance of the TTA could be further improved by constructing a micro/nanostructure on the surface of the PTFE film and optimizing the experimental process, such as ensuring the smoothness of the PTFE film to realize physically full contact with the Cu pad. Apart from pixels covered by the letter, some pixels next to the covered area were also affected to a different degree, which could be reasonably interpreted as the influence of potential distribution between the PTFE film and the Cu pad on these adjoining pixels, like pixel R3-C7 in Figure S3b. Nevertheless, C-, A-, and S-shaped images could be distinctly recognized, manifesting its bright prospects in real-time tactile sensing and image reconstruction. Moreover, the sensing array can be packaged by integrating the PTFE film into the system. With this design (detailed integration process is introduced in Methods and Figure S7), the tactile sensors are able to produce stable output signals whatever the touching objects are, therefore enlarging its application range.

CONCLUSIONS

In summary, this work presents a flexible substrate-based TTA as a large-scale and active tactile sensing system. Utilizing the electrostatic potential created by the triboelectrification, the I_{DS} of each transistor unit can be modulated for sensing the external mechanical stimuli. Unlike the proposed sensor arrays before, with complicated and high-cost fabrication procedures,

DOI: 10.1021/acsnano.6b05507
ACS Nano XXXX, XXX, XXX–XXX

the flexible TTA combines traditional electronic devices with cheap but practical polymer films for contact electrification to achieve real-time high sensing and dynamic mapping. By investigating in detail the electrical characteristics of pixels, we demonstrated the TTA's durability, independence, and synchronicity. Moreover, the pixel can even be scaled down to the size of 0.5 × 0.5 mm^2 while maintaining good sensitivity and thus realizing a high resolution of the TTA. Single- and multiple-point touch map reconstruction, motion monitoring, and trajectory recording have been successfully accomplished, all of which verifies the outstanding performances of the TTA. Relying on the core concepts of tribotronics, in the future, more electronics and modules could be included to construct a multifunctional system that not only allows tactile sensing but also enables many other intelligent and significant functionalities. It is anticipated that the TTA can unlock a door to a broad range of applications in wearable electronics, human–machine interfaces, and personalized health monitoring.

METHODS

Fabrication of the Flexible TTA. A polyimide (PI) substrate (100 μm in thickness) was first cleaned with deionized water, ethanol, and acetone and was then blown dry. The PI substrate was treated at 120 °C for 30 min. Localized via holes were drilled on the PI substrate, and subsequently, 10 μm thick Cu was deposited onto the selective area of both sides of the PI substrate to serve as electrical wires. Accordingly, 10 Cu electrodes in rows and 10 Cu electrodes in columns with a width of 250 μm were patterned on the top and bottom layer of the PI substrate, respectively. Later, a layer of Ni (3 μm) was electroplated on the top layer of the substrate according to the designed circuit configuration to form pads with the size of 5 × 5 mm^2, followed by the deposition of Cu (0.25 μm) to the corresponding area of electrically plated nickel. As a final step, chips of microfabricated n-type transistors and diodes based on a standard silicon process were integrated onto the as-fabricated PI substrate. All the gate electrodes of the transistors were bonded to the defined Cu pad area through the via hole, while the 100 drain electrodes and source electrodes were bonded to the patterned Cu wire electrodes. With such a design, each pixel is independent of any other pixels. To integrate the mobile electrification layer into the as-fabricated device, the freestanding PTFE film was first adhered to another flexible PI substrate, and then the Cu pad and the PTFE film were separated by spacers (3M 4-4100 adhesive). After these spacers were placed, the whole device was sealed by adhesive tape.

Electrical Characterization of the TTA. Drain–source currents and sensing characteristics of single pixels were determined using a digital multimeter (Agilent 34411A), a DC power supply (Rek RPS6003D-2), and manual translation stages (NFP-3462) under ambient condition at room temperature. A source meter (2612B, Keithley) was used to characterize the transfer and output characteristics of the transistor. To test the durability of the TTA, a stepping motor (XRV76) was used to supply a periodical reciprocating motion at speed of 20 mm/s. All of the 100 pixels in the TTA were addressed individually by iteratively switching a 128 channel multiplexer matrix (PXI-2530, PXI-2630B, National Instrument). The output current signals from each pixel in the TTA were measured and averaged using a $6^1/_2$-digit digital multimeter (PXI-4072, National Instrument), and a constant bias (V_{DS}) was provided by a programmable DC power supply (PXI-4110, National Instrument). A homemade data acquisition system was utilized to record and process the output current signals of the fabricated TTA in real time and then to reconstruct the two-dimensional intensity map of the TTA under different external stimuli.

ASSOCIATED CONTENT

Supporting Information

The Supporting Information is available free of charge on the ACS Publications website at DOI: 10.1021/acsnano.6b05507.

Figures S1–S7 (PDF)

Video S1: tribotronic transistor array for multipoint tactile sensing (AVI)

Video S2: tribotronic transistor array for dynamic motion monitoring (AVI)

Video S3: tribotronic transistor array for real-time trajectory recording (AVI)

AUTHOR INFORMATION

Corresponding Authors

*E-mail: czhang@binn.cas.cn.

*E-mail: zlwang@gatech.edu.

ORCID

Zhong Lin Wang: 0000-0002-5530-0380

Notes

The authors declare no competing financial interest.

ACKNOWLEDGMENTS

The authors thank the National Natural Science Foundation of China (Nos. 51475099 and 51432005), Beijing Natural Science Foundation (No. 4163077), the Youth Innovation Promotion Association, CAS, the "thousands talents" program for the pioneer researcher and his innovation team, China, and National Key Research and Development Program of China (2016YFA0202704) for support.

REFERENCES

(1) Mannsfeld, S. C. B.; Tee, B. C.-K.; Stoltenberg, R. M.; Chen, C. V. H.-H.; Barman, S.; Muir, B. V. O.; Sokolov, A. N.; Reese, C.; Bao, Z. Highly Sensitive Flexible Pressure Sensors with Microstructured Rubber Dielectric Layers. *Nat. Mater.* **2010**, *9*, 859–864.

(2) Wang, C.; Hwang, D.; Yu, Z.; Takei, K.; Park, J.; Chen, T.; Ma, B.; Javey, A. User-Interactive Electronic Skin for Instantaneous Pressure Visualization. *Nat. Mater.* **2013**, *12*, 899–904.

(3) Hammock, M. L.; Chortos, A.; Tee, B. C.-K.; Tok, J. B.-H.; Bao, Z. 25th Anniversary Article: the Evolution of Electronic Skin (E-Skin): A Brief History, Design Considerations, and Recent Progress. *Adv. Mater.* **2013**, *25*, 5997–6038.

(4) Chortos, A.; Bao, Z. Skin-Inspired Electronic Devices. *Mater. Today* **2014**, *17*, 321–331.

(5) Kaltenbrunner, M.; Sekitani, T.; Reeder, J.; Yokota, T.; Kuribara, K.; Tokuhara, T.; Drack, M.; SchwÖdiauer, R.; Graz, I.; Bauer-Gogonea, S.; Bauer, S.; Someya, T. An Ultra-Lightweight Design for Imperceptible Plastic Electronics. *Nature* **2013**, *499*, 458–463.

(6) Kim, D.-H.; Lu, N.; Ma, R.; Kim, Y.-S.; Kim, R.-H.; Wang, S.; Wu, J.; Won, S. M.; Tao, H.; Islam, A.; Yu, K. J.; Kim, T.-I.; Chowdhury, R.; Ying, M.; Xu, L.; Li, M.; Chung, H.-J.; Keum, H.; McCormick, M.; Liu, P.; Zhang, Y.-W.; Omenetto, F. G.; Huang, Y.; Coleman, T.; Rogers, J. A. Epidermal Electronics. *Science* **2011**, *333*, 838–843.

(7) Harada, S.; Kanao, K.; Yamamoto, Y.; Arie, T.; Akita, S.; Takei, K. Fully Printed Flexible Fingerprint-Like Three-Axis Tactile and Slip Force and Temperature Sensors for Artificial Skin. *ACS Nano* **2014**, *8*, 12851–12857.

(8) Viry, L.; Levi, A.; Totaro, M.; Mondini, A.; Mattoli, V.; Mazzolai, B.; Beccai, L. Flexible Three-Axial Force Sensor for Soft and Highly Sensitive Artificial Touch. *Adv. Mater.* **2014**, *26*, 2659–2664.

(9) Takei, K.; Takahashi, T.; Ho, J. C.; Ko, H.; Gillies, A. G.; Leu, P. W.; Fearing, R. S.; Javey, A. Nanowire Active-Matrix Circuitry for Low-Voltage Macroscale Artificial Skin. *Nat. Mater.* **2010**, *9*, 821–826.

DOI: 10.1021/acsnano.6b05507
ACS Nano XXXX, XXX, XXX–XXX

(10) Wu, W.; Wen, X.; Wang, Z. L. Taxel-Addressable Matrix of Vertical-Nanowire Piezotronic Transistors for Active and Adaptive Tactile Imaging. *Science* **2013**, *340*, 952−957.
(11) Lee, S.; Reuveny, A.; Reeder, J.; Lee, S.; Jin, H.; Liu, Q.; Yokota, T.; Sekitani, T.; Isoyama, T.; Abe, Y.; Suo, Z.; Someya, T. A Transparent Bending-Insensitive Pressure Sensor. *Nat. Nanotechnol.* **2016**, *11*, 472−478.
(12) Chou, H.-H.; Nguyen, A.; Chortos, A.; To, J. W.F.; Lu, C.; Mei, J.; Kurosawa, T.; Bae, W.-G.; Tok, J. B.-H.; Bao, Z. A Chameleon-Inspired Stretchable Electronic Skin with Interactive Colour Changing Controlled by Tactile Sensing. *Nat. Commun.* **2015**, *6*, 8011.
(13) Pan, L.; Chortos, A.; Yu, G.; Wang, Y.; Isaacson, S.; Allen, R.; Shi, Y.; Dauskardt, R.; Bao, Z. An Ultra-Sensitive Resistive Pressure Sensor Based on Hollow-Sphere Microstructure Induced Elasticity in Conducting Polymer Film. *Nat. Commun.* **2014**, *5*, 3002.
(14) Zang, Y.; Zhang, F.; Huang, D.; Gao, X.; Di, C.-A.; Zhu, D. Flexible Suspended Gate Organic Thin-Film Transistors for Ultra-Sensitive Pressure Detection. *Nat. Commun.* **2015**, *6*, 6269.
(15) Sun, Q.; Kim, D. H.; Park, S. S.; Lee, N. Y.; Zhang, Y.; Lee, J. H.; Cho, K.; Cho, J. H. Transparent, Low-Power Pressure Sensor Matrix Based on Coplanar-Gate Graphene Transistors. *Adv. Mater.* **2014**, *26*, 4735−4740.
(16) Hong, S. Y.; Lee, Y. H.; Park, H.; Jin, S. W.; Jeong, Y. R.; Yun, J.; You, I.; Zi, G.; Ha, J. S. Stretchable Active Matrix Temperature Sensor Array of Polyaniline Nanofibers for Electronic Skin. *Adv. Mater.* **2016**, *28*, 930−935.
(17) Ren, X.; Pei, K.; Peng, B.; Zhang, Z.; Wang, Z.; Wang, X.; Chan, P. K.L. A Low-Operating-Power and Flexible Active-Matrix Organic-Transistor Temperature-Sensor Array. *Adv. Mater.* **2016**, *28*, 4832−4838.
(18) Schwartz, G.; Tee, B. C.-K.; Mei, J.; Appleton, A. L.; Kim, D. H.; Wang, H.; Bao, Z. Flexible Polymer Transistors with High Pressure Sensitivity for Application in Electronic Skin and Health Monitoring. *Nat. Commun.* **2013**, *4*, 1859.
(19) Takahashi, T.; Takei, K.; Gillies, A. G.; Fearing, R. S.; Javey, A. Carbon Nanotube Active-Matrix Backplanes for Conformal Electronics and Sensors. *Nano Lett.* **2011**, *11*, 5408−5413.
(20) Yun, S.; Park, S.; Park, B.; Kim, Y.; Park, S. K.; Nam, S.; Kyung, K.-U. Polymer-Waveguide-Based Flexible Tactile Sensor Array for Dynamic Response. *Adv. Mater.* **2014**, *26*, 4474−4480.
(21) Zang, Y.; Zhang, F.; Huang, D.; Di, C.-A.; Zhu, D. Sensitive Flexible Magnetic Sensors Using Organic Transistors with Magnetic-Functionalized Suspended Gate Electrodes. *Adv. Mater.* **2015**, *27*, 7979−7985.
(22) Alfadhel, A.; Kosel, J. Magnetic Nanocomposite Cilia Tactile Sensor. *Adv. Mater.* **2015**, *27*, 7888−7892.
(23) Sun, Q.; Seung, W.; Kim, B. J.; Seo, S.; Kim, S.-W.; Cho, J. H. Active Matrix Electronic Skin Strain Sensor Based on Piezopotential-Powered Graphene Transistors. *Adv. Mater.* **2015**, *27*, 3411−3417.
(24) Park, J.; Lee, Y.; Hong, J.; Lee, Y.; Ha, M.; Jung, Y.; Lim, H.; Kim, S. Y.; Ko, H. Tactile-Direction-Sensitive and Stretchable Electronic Skins Based on Human-Skin-Inspired Interlocked Microstructures. *ACS Nano* **2014**, *8*, 12020−12029.
(25) Harada, S.; Honda, W.; Arie, T.; Akita, S.; Takei, K. Fully Printed, Highly Sensitive Multifunctional Artificial Electronic Whisker Arrays Integrated with Strain and Temperature Sensors. *ACS Nano* **2014**, *8*, 3921−3927.
(26) Gong, S.; Schwalb, W.; Wang, Y.; Chen, Y.; Tang, Y.; Si, J.; Shirinzadeh, B.; Cheng, W. A Wearable and Highly Sensitive Pressure Sensor with Ultrathin Gold Nanowires. *Nat. Commun.* **2014**, *5*, 3132.
(27) Chen, L. Y.; Tee, B. C.-K.; Chortos, A. L.; Schwartz, G.; Tse, V.; Lipomi, D. J.; Wong, H.-S. P.; McConnell, M. V.; Bao, Z. Continuous Wireless Pressure Monitoring and Mapping with Ultra-Small Passive Sensors for Health Monitoring and Critical Care. *Nat. Commun.* **2014**, *5*, 5028.
(28) Fan, F. R.; Tian, Z.-Q.; Wang, Z. L. Flexible Triboelectric Generator. *Nano Energy* **2012**, *1*, 328−334.
(29) Zhang, C.; Tang, W.; Han, C. B.; Fan, F. R.; Wang, Z. L. Theoretical Comparison, Equivalent Transformation and Conjunction Operations of Electromagnetic Induction Generator and Triboelectric Nanogenerator for Harvesting Mechanical Energy. *Adv. Mater.* **2014**, *26*, 3580−3591.
(30) Fan, F.; Tang, W.; Yao, Y.; Luo, J.; Zhang, C.; Wang, Z. L. Complementary Power Output Characteristics of Electromagnetic Generators and Triboelectric Generators. *Nanotechnology* **2014**, *25*, 135402.
(31) Tang, W.; Zhou, T.; Zhang, C.; Fan, F. R.; Han, C. B.; Wang, Z. L. A Power-Transformed-and-Managed Triboelectric Nanogenerator and Its Applications in A Self-Powered Wireless Sensing Node. *Nanotechnology* **2014**, *25*, 225402.
(32) Yang, Y.; Zhang, H.; Lin, Z.-H.; Zhou, Y. S.; Jing, Q.; Su, Y.; Yang, J.; Chen, J.; Hu, C.; Wang, Z. L. Human Skin Based Triboelectric Nanogenerators for Harvesting Biomechanical Energy and as Self-Powered Active Tactile Sensor System. *ACS Nano* **2013**, *7*, 9213−9222.
(33) Li, X. H.; Han, C. B.; Jiang, T.; Zhang, C.; Wang, Z. L. A Ball-Bearing Structured Triboelectric Nanogenerator for Nondestructive Damage and Rotating Speed Measurement. *Nanotechnology* **2016**, *27*, 085401.
(34) Wang, X.; Zhang, H.; Dong, L.; Han, X.; Du, W.; Zhai, J.; Pan, C.; Wang, Z. L. Self-Powered High-Resolution and Pressure-Sensitive Triboelectric Sensor Matrix for Real-Time Tactile Mapping. *Adv. Mater.* **2016**, *28*, 2896−2903.
(35) Han, C. B.; Zhang, C.; Li, X. H.; Zhang, L.; Zhou, T.; Hu, W.; Wang, Z. L. Self-Powered Velocity and Trajectory Tracking Sensor Array Made of Planar Triboelectric Nanogenerator Pixels. *Nano Energy* **2014**, *9*, 325−333.
(36) Pang, Y. K.; Li, X. H.; Chen, M. X.; Han, C. B.; Zhang, C.; Wang, Z. L. Triboelectric Nanogenerators as A Self-Powered 3D Acceleration Sensor. *ACS Appl. Mater. Interfaces* **2015**, *7*, 19076−19082.
(37) Zhang, L. M.; Xue, F.; Du, W.; Han, C. B.; Zhang, C.; Wang, Z. L. Transparent Paper-Based Triboelectric Nanogenerator as A Page Mark and Anti-Theft Sensor. *Nano Res.* **2014**, *7*, 1215−1223.
(38) Zhang, C.; Wang, Z. L. Tribotronics—A New Field by Coupling Triboelectricity and Semiconductor. *Nano Today* **2016**, *11*, 521−536.
(39) Zhang, C.; Tang, W.; Zhang, L.; Han, C.; Wang, Z. L. Contact Electrification Field-Effect Transistor. *ACS Nano* **2014**, *8*, 8702−8709.
(40) Wu, J. M.; Lin, Y. H.; Yang, B. Z. Force-Pad Made from Contact-Electrification Poly (Ethylene Oxide)/InSb Field-Effect Transistor. *Nano Energy* **2016**, *22*, 468−474.
(41) Zhang, C.; Tang, W.; Pang, Y.; Han, C.; Wang, Z. L. Active Micro-Actuators for Optical Modulation Based on A Planar Sliding Triboelectric Nanogenerator. *Adv. Mater.* **2015**, *27*, 719−726.
(42) Zhang, C.; Zhang, L. M.; Tang, W.; Han, C. B.; Wang, Z. L. Tribotronic Logic Circuits and Basic Operations. *Adv. Mater.* **2015**, *27*, 3533−3540.
(43) Li, J.; Zhang, C.; Duan, L.; Zhang, L. M.; Wang, L. D.; Dong, G. F.; Wang, Z. L. Flexible Organic Tribotronic Transistor Memory for A Visible and Wearable Touch Monitoring System. *Adv. Mater.* **2016**, *28*, 106−110.
(44) Zhang, C.; Li, J.; Han, C. B.; Zhang, L. M.; Chen, X. Y.; Wang, L. D.; Dong, G. F.; Wang, Z. L. Organic Tribotronic Transistor for Contact-Electrification-Gated Light-Emitting Diode. *Adv. Funct. Mater.* **2015**, *25*, 5625−5632.
(45) Pang, Y.; Xue, F.; Wang, L.; Chen, J.; Luo, J.; Jiang, T.; Zhang, C.; Wang, Z. L. Tribotronic Enhanced Photoresponsivity of A MoS_2 phototransistor. *Adv. Sci.* **2016**, *3*, 1500419.
(46) Zhang, C.; Zhang, Z. H.; Yang, X.; Zhou, T.; Han, C. B.; Wang, Z. L. Tribotronic Phototransistor for Enhanced Photodetection and Hybrid Energy Harvesting. *Adv. Funct. Mater.* **2016**, *26*, 2554−2560.
(47) Xue, F.; Chen, L.; Wang, L.; Pang, Y.; Chen, J.; Zhang, C.; Wang, Z. L. MoS_2 Tribotronic Transistor for Smart Tactile Switch. *Adv. Funct. Mater.* **2016**, *26*, 2104−2109.
(48) Niu, S.; Liu, Y.; Wang, S.; Lin, L.; Zhou, Y. S.; Hu, Y.; Wang, Z. L. Theoretical Investigation and Structural Optimization of Single-Electrode Triboelectric Nanogenerators. *Adv. Funct. Mater.* **2014**, *24*, 3332−3340.

DOI: 10.1021/acsnano.6b05507
ACS Nano XXXX, XXX, XXX−XXX

(49) Niu, S.; Wang, S.; Lin, L.; Liu, Y.; Zhou, Y. S.; Hu, Y.; Wang, Z. L. Theoretical Study of Contact-Mode Triboelectric Nanogenerators as an Effective Power Source. *Energy Environ. Sci.* **2013**, *6*, 3576−3583.

DOI: 10.1021/acsnano.6b05507
ACS Nano XXXX, XXX, XXX−XXX